Tailoring the sensing capabilities of nanohole arrays in gold films with Rayleigh anomaly-surface plasmon polaritons

Jeffrey M. McMahon[1,2], Joel Henzie[2], Teri W. Odom[2,3], George C. Schatz[2], and Stephen K. Gray[1*]

[1] *Chemistry Division and Center for Nanoscale Materials, Argonne National Laboratory, Argonne, Illinois 60439, USA*
[2] *Department of Chemistry, Northwestern University, 2145 Sheridan Road, Evanston, Illinois 60208, USA*
[3] *Materials Science and Engineering, Northwestern University, 2200 Campus Drive, Evanston, Illinois 60208, USA*
**Corresponding author: gray@tcg.anl.gov*

Abstract: Surface plasmon polaritons (SPPs) and diffraction effects such as Rayleigh anomalies (RAs) play key roles in the transmission of light through periodic subwavelength hole arrays in metal films. Using a combination of theory and experiment we show how refractive index (RI) sensitive transmission features arise from hole arrays in thin gold films. We show that large transmission amplitude changes occur over a narrow range of RI values due to coupling between RAs and SPPs on opposite sides of the metal film. Furthermore, we show how to predict, on the basis of a relatively simple analysis, the periodicity and other system parameters that should be used to achieve this **"**RA-SPP" effect for any desired RI range.

OCIS codes: (240.6680) Surface plasmons; (050.6624) Subwavelength structures; (260.3910) Metal optics; (050.1220) Apertures; (280.4788) Optical sensing and sensors; (290.3030) Index measurements

References and links

1. T. W. Ebbesen, H. J. Lezec, H. F. Ghaemi, T. Thio, and P. A. Wolff, "Extraordinary optical transmission through sub-wavelength hole arrays," Nature (London) **391**, 667 – 669 (1998).
2. H. F. Ghaemi, T. Thio, D. E. Grupp, T. W. Ebbesen, and H. J. Lezec, "Surface plasmons enhance optical transmission through subwavelength holes," Phys. Rev. B **58**, 6779-6782 (1998).
3. S.-H. Chang, S. K. Gray and G. C. Schatz, "Surface plasmon generation and light transmission by isolated nanoholes and arrays of nanoholes in thin metal films," Opt. Express **13**, 3150 – 3165 (2005). http://www.opticsinfobase.org/abstract.cfm?URI=oe-13-8-3150.
4. M. M. J. Treacy, "Dynamical diffraction explanation of the anomalous transmission of light through metallic gratings," Phys. Rev. B **66**, 195105 (11 pages) (2002).
5. M. Sarrazin, J.-P. Vigneron, and J.-M. Vigoureux, "Role of Wood anomalies in optical properties of thin metallic films with a bidimensional array of subwavelength holes," Phys. Rev. B **67**, 085415 (8 pages) (2003).
6. Z. Ruan and M. Qiu, "Enhanced Transmission through Periodic Arrays of Subwavelength Holes: The Role of Localized Waveguide Resonances," Phys. Rev. Lett. **96**, 233901 (4 pages) (2006).
7. C. Genet, M. P. van Exter, J. P. Woerdman, "Fano-type interpretation of red shifts and red tails in hole array transmission spectra," Opt. Commun. **225**, 331 – 336 (2003).
8. M. E. Stewart, N. H. Mack, V. Malyarchuk, J. A. N. T. Soares, T.-W. Lee, S. K. Gray, R. G. Nuzzo, and J. A. Rogers, "Quantitative multispectral biosensing and 1D imaging using quasi-3D plasmonic crystals," Proc. Nat. Acad. Sci. (USA) **103**, 17143 – 17148 (2006).
9. A. Taflove and S. Hagness, *Computational Electrodynamics: The Finite-Difference Time-Domain Method*, 3rd Edition (Artech House, Mass., 2005).
10. T. W. Lee, S. K. Gray, "Subwavelength light bending by metal slit structures," Opt. Express **13**, 9652 – 9659 (2005). http://www.opticsinfobase.org/abstract.cfm?URI=oe-13-24-9652.
11. A. Benabbas, V. Halte, and J.-Y. Bigot, "Analytical model of the optical response of periodically structured metallic films," Opt. Express **13**, 8730 – 8745 (2005). http://www.opticsinfobase.org/abstract.cfm?URI=oe-13-22-8730.

#86022 - $15.00 USD Received 1 Aug 2007; revised 15 Nov 2007; accepted 16 Nov 2007; published 19 Dec 2007

12. J. Henzie, M. H. Lee, T. W. Odom, "Multiscale Patterning of Plasmonic Metamaterials," Nature Nanotech. **2**, 549-554 (2007).
13. A. Hessel and A. A. Oliner, "A New Theory of Wood's Anomalies on Optical Gratings," Appl. Opt. **4**, 1275-1297 (1965).
14. S. Darmanyan, M. Neviere, and A. Zayats, "Analytical theory of optical transmission through periodically structured metallic films via tunnel-coupled surface polariton modes," Phys. Rev. B **70**, 075103 (9 pages) (2004).
15. J. Steele, C. Moran, C. Aguirre, A. Lee, N. Halas, "Metallodielectric gratings with subwavelength slots: Optical properties," Phys. Rev. B **68**, 205103 (7 pages) (2003).
16. P. R. H. Stark, A. E. Halleck, D. N. Larson, "Short order nanohole arrays in metals for highly sensitive probing of local indices of refraction as the basis for a highly multiplexed biosensor technology," Methods **37**, 37–47 (2005).

1. Introduction

Light transmission through subwavelength diameter holes in metal films has been the focus of much research since the pioneering work of Ebbesen *et al.* [1], and the mechanisms underlying the enhanced or extraordinary optical transmission in these systems have been the subject of much discussion. Important influences on transmission include: surface plasmon polaritons (SPPs), diffractive effects including Rayleigh anomalies (RAs), and localized waveguide modes [1-7]. Recently, for example, a variety of these features were attributed to the large refractive index (RI) sensitivities observed in gold films deposited on arrays of 500 nm wells molded in a polymer substrate [8].

In this paper we show how certain narrow spectroscopic features in the light transmission through a periodic array of holes in a thin gold film can be described by coupling a RA on one side of the film with a SPP Bloch wave (SPP-BW) on the opposite side. Both rigorous computational electrodynamics modeling and experiment are used to study this "RA-SPP" effect. For the system studied, we find that it can lead to large increases in transmission amplitudes with respect to RI unit (RIU) of a substrate, up to 150%/RIU, because of strong coupling between the opposite sides of a thin metal film. Furthermore, we show that relatively simple equations can be used to predict the periodicity of the array and the index of the supporting substrate in order to achieve optimal sensing characteristics for a specified substrate RI.

2. Methods

We consider a square array of nanoholes of periodicity P in a gold film sandwiched between dielectric materials I and III (Fig. 1). Material I (bottom) is taken to be the supporting material for the film, and material III (top) is a variable index substrate, e.g. some liquid or solution. Light is incident from region I and the transmission spectrum is obtained in region III.

2.1 Theoretical methods

The three-dimensional finite-difference time-domain (FDTD) [3, 9] method is used to model the system in Fig. 1, which consists of modeling a single unit cell (a P x P square in the xy-plane centered on a hole) with appropriate periodic boundary conditions and with absorbing layers placed in the lower and upper regions of z. Grid spacings of $\Delta x = \Delta y = \Delta z = 4$ nm are used and a total simulation time of 250 x 10^{-15} s is employed. Test calculations with somewhat larger grid spacings and shorter simulation times indicate that the results obtained are sufficiently converged. Incident light is introduced into the computational domain using the total field / scattered field formulation 500 nm below the bottom surface of the film, and is modeled as a 600 nm sinusoidal pulse polarized along the x-axis and damped by a Gaussian

#86022 - $15.00 USD Received 1 Aug 2007; revised 15 Nov 2007; accepted 16 Nov 2007; published 19 Dec 2007

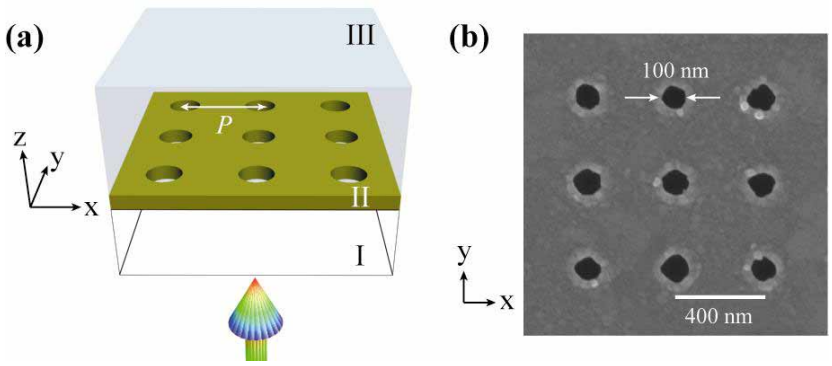

Fig. 1. Hole array system under study showing (a) schematic representation and (b) SEM image. Light is incident from region I towards a thin gold film (region II), perforated with a square array of nanoholes, and the transmission spectrum is obtained in region III.

function centered at t_0 = 100 x 10^{-15} s with a width of τ = 1.20 x 10^{-15} s. The gold film is assumed to have a wavelength-dependent dielectric constant, $\varepsilon_{Au}(\lambda)$, corresponding to a Drude plus two-pole Lorentz form used in Ref. [8] with Drude parameters ε_∞ = 5.40, γ_D = 0.103 x 10^{15} Hz, and ω_D = 0.140 x 10^{17} Hz and Lorentz parameters ω_{L1} = 0.427 x 10^{16} Hz and ω_{L2} = 0.523 x 10^{16} Hz, γ_{L1} = 0.870 x 10^{15} Hz and γ_{L2} = 1.32 x 10^{15} Hz, g_{L1} = 0.268 and g_{L1} = 0.732, and $\Delta\varepsilon$ = 2.54. See Ref. [10] for details on how such a model is implemented within the FDTD structure.

The desired transmission spectra are for zero-order transmission, i.e. they do not include contributions from light scattered away from the incident direction. To obtain this result theoretically we calculate the Fourier transformed time-evolving electric and magnetic fields, $\mathbf{E}(x, y, \lambda)$ and $\mathbf{H}(x, y, \lambda)$, on an *xy*-plane z_T = 700 nm above the top surface of film. It is then necessary to project out only the zero-order scattering contributions from these fields. Since the wave vector for zero-order scattering is $\mathbf{k} = \hat{\mathbf{x}}\ 0 + \hat{\mathbf{y}}\ 0 + \hat{\mathbf{z}}\ (\omega/c)$ and *z* is fixed for a given *xy*-plane of interest, the relevant projections of the fields are simply proportional to integrating them over *x* and *y*. If $\mathbf{E}_0(z_T, \lambda)$ and $\mathbf{H}_0(z_T, \lambda)$ denote these projections then the zero-order transmission is given by $T(\lambda) = P_T(\lambda) / P_{inc}(\lambda)$ with $P_T(\lambda) = (1/2)\ \mathrm{Re}\ (\mathbf{E}_0 \times \mathbf{H}_0^*)_z$. The quantity $P_{inc}(\lambda)$ is the incident flux calculated in the same way.

A difficulty with the FDTD calculations is that they are very computationally demanding. In order to obtain an idea of how the RA-SPP effect might be affected by variations in system parameters, more numerically efficient two-dimensional rigorous coupled-wave analysis (RCWA) calculations are also carried out using the model of Ref. [11] for scattering of TM polarized light by a metal grating. Since it is a 2D model it is actually a model of periodic slits as opposed to holes. Furthermore, only zero and first order Fourier components are used for the metallic dielectric constant and so it is not, strictly, even an exact solution of the 2D problem. However, we find that the model still captures important features consistent with the transmission trends for (1, 0) SPP-BWs and (1, 0) RAs. In addition, RCWA allows specific diffraction orders to be independently studied.

2.2 Experimental methods

Experimental transmission measurements are obtained using an inverted optical microscope by passing collimated white light (100 W halogen source) under normal excitation through the gold nanohole film supported on a glass (bottom) substrate (RI = 1.52). The transmitted light is collected through a 100x objective (NA = 0.5) and then focused onto an imaging spectrometer [12]. The (top) substrate RI is varied by placing a drop of immersion liquid (Cargille Labs) between the gold film and the objective.

#86022 - $15.00 USD Received 1 Aug 2007; revised 15 Nov 2007; accepted 16 Nov 2007; published 19 Dec 2007

3. Results and discussion

3.1 The RA-SPP effect: General considerations

An approximate equation for the free-space incident wavelength that excites a SPP-BW, λ_{SPP}, is [2, 3]:

$$\lambda_{SPP} = \frac{P}{\left(s_1^2 + s_2^2\right)^{1/2}} \, \mathrm{Re}\left(\frac{\varepsilon_{Au}(\lambda_{SPP}) \, \varepsilon_X}{\varepsilon_{Au}(\lambda_{SPP}) + \varepsilon_X}\right)^{1/2} , \qquad (1)$$

and the relation for the free-space incident wavelength of a RA, λ_{RA}, is

$$\lambda_{RA} = \frac{P}{\left(w_1^2 + w_2^2\right)^{1/2}} \, n_X , \qquad (2)$$

where (s_1, s_2) and (w_1, w_2) are integer pairs that correspond to the particular order of the SPP-BW or RA, ε_X is the real, relative dielectric constant of medium X = I or III ($n_X = \varepsilon_X^{1/2}$), and $\varepsilon_{Au}(\lambda)$ is the complex wavelength-dependent dielectric constant of gold. Note that the positions associated with Eq. (1) are approximate because coupling between top and bottom resonances is ignored. One expects this equation to be most accurate when the metal film is thick and/or n_I and n_{III} differ substantially so that the resonances do not interact. In thin metal films when n_I and n_{III} become similar (ca. $\Delta n < 0.2$), the actual positions of the SPP-BW resonance features are red or blue-shifted slightly relative to Eq. (1) (see below). RAs, however, are non-resonant spectral features associated with gratings.

The RA, Eq. (2), occurs at the threshold of a diffraction order and corresponds to light being diffracted at an angle parallel to the metal surface. It is also sometimes referred to as a Wood anomaly [2, 3]. However, it is important to keep in mind that, following the detailed analysis and classification of Wood anomalies by Hessel and Oliner [13], the RA is one of two types of Wood anomalies. The *other* type of Wood anomaly identified by them is a "resonant" anomaly, which could be a SPP-BW, waveguide mode, or possibly a hybrid mode. In their terminology, the RA-SPP, the main topic of this paper, can be viewed as a particular type of resonant Wood anomaly, since it is a hybrid of a RA and a SPP-BW.

Figure 2 shows how the positions of SPP-BWs and RAs predicted by Eqs. (1) and (2) evolve as n_{III} is changed while $n_I = 1.52$ and $P = 400$ nm remain fixed. Only the first order (s_1, s_2) = (w_1, w_2) = (1, 0) cases are shown since they are the strongest features in this wavelength range and for this P. The crossing point labeled as RA-SPP corresponds to where the (1, 0) n_{III} RA and the (1, 0) n_I SPP-BW coexist and can interact if the metal film is thin enough, which we show below leads to a strong variation in transmission amplitude for film thicknesses up to 65 nm.

The other crossing points in Fig. 2 lead to couplings that are less relevant for obtaining narrow spectral features that are especially sensitive to variations of n_{III}. The coupling of the two SPP-BWs features near $n_{III} = 1.52$ will lead to a broader peak than the RA-SPP peak since SPP-BWs are intrinsically broader than the RAs due to their finite lifetimes. (We will show, however, that the hybridization that results from this interaction plays a role in the RA-SPP effect.) The crossing of the two RA features could produce narrow structures, but its effect is overwhelmed by SPP-BW coupling near the same wavelength. Finally, the (1, 0) n_{III} SPP-BW and (1, 0) n_I RA crossing near $n_{III} = 1.35$ occurs in a wavelength region where higher order SPP-BWs, localized resonances, and direct transmission can all be important.

#86022 - $15.00 USD Received 1 Aug 2007; revised 15 Nov 2007; accepted 16 Nov 2007; published 19 Dec 2007

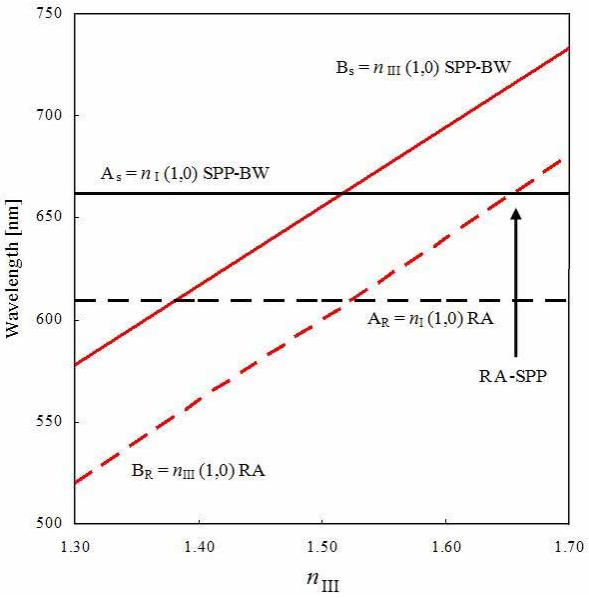

Fig. 2. Zero-order positions of (1, 0) SPP-BWs and RAs [Eqs. (1) and (2)] as a function n_{III} for $n_I = 1.52$ and $P = 400$ nm. The n_I SPP-BWs and RAs are denoted A_S and A_R, and the n_{III} SPP-BWs and RAs as B_S and B_R.

Using Eqs. (1) and (2) It is possible to design a nanohole array system exhibiting a RA-SPP falling in some desired RI sensing range. If we equate the first order SPP-BW condition, $(s_1, s_2) = (1, 0)$, on the bottom substrate (n_I) with the first order RA condition, $(w_1, w_2) = (1, 0)$, on the top substrate (n_{III}), we obtain the simple relation:

$$n_{III} = \mathrm{Re}\left(\frac{\varepsilon_{Au}(\lambda_{RA\text{-}SPP})\varepsilon_I}{\varepsilon_{Au}(\lambda_{RA\text{-}SPP}) + \varepsilon_I} \right)^{1/2} \quad , \tag{3}$$

which, like Eq. (1), is an implicit relation for a wavelength. In this case, the wavelength $\lambda_{RA\text{-}SPP}$ is where the zero-order SPP-BW and RA conditions are the same. The required periodicity for the hole array at this crossing point is then found from:

$$P = \lambda_{RA\text{-}SPP}/n_{III} \quad . \tag{4}$$

To achieve sensing for RI values near some specific n_{III} value, Eq. (3) is first rewritten as a root equation, $f(\lambda_{RA\text{-}SPP}) = 0$, and solved using bisection for $\lambda_{RA\text{-}SPP}$. Then Eq. (4) is used to determine the necessary P. For example, with a glass supporting substrate ($n_I = 1.52$) and targeting RI values near $n_{III} = 1.65$, $\lambda_{RA\text{-}SPP} \approx 650$ nm and $P \approx 400$ nm. Of course, from the discussion above, we expected this result. More importantly, we can use Eqs. (3) and (4) to target other RI ranges. For example, to target $n_{III} = 1.75$ we find $P \approx 333$ nm. It turns out that RA-SPP solutions exist only for target n_{III} values in a small range $n_I < n_{III} < n_I + \Delta$, where Δ depends on the nature of the metal and n_I (e.g. $\Delta \approx 0.35$ for gold with $n_I = 1.52$). To design a system sensitive to $n_{III} = 1.40$, for example, it would therefore be necessary to use a supporting substrate with $n_I < 1.40$.

3.2 Transmission spectra

We now present evidence for the picture outlined above by focusing on a 50 nm thick gold film, perforated with a $P = 400$ nm arrays of holes of diameter 100 nm, and supported on glass ($n_I = 1.52$). Figure 3 displays zero-order transmission spectra, FDTD and experimental, for $n_{III} = 1.00$ - 1.40 (regime where $n_{III} < n_I$), and Fig. 4 shows results for $n_{III} = 1.50$ - 1.70.

#86022 - $15.00 USD Received 1 Aug 2007; revised 15 Nov 2007; accepted 16 Nov 2007; published 19 Dec 2007

These figures include labels of the relevant minima (described in detail below) with the approximate SPP-BW or RA assignments from Fig. 2. Note that the predicted higher order (1, 1) n_{III} SPP-BW (not shown in Fig. 2) is labeled as C. The level of agreement between experiment and theory is reasonable in terms of positions of the minima and maxima, and overall trends. However, there are some quantitative differences in the magnitudes of the largest transmission peaks, which are most likely due to small, but very sensitive, deviations between the experimental hole array structures and the theoretical idealized configurations [8]. We find, for example, that if the diameter of the holes is increased to 120 nm, then the calculated transmission amplitude of the longest wavelength peak nearly doubles. Although the experimental holes have, on average, 100 nm diameters, slight size differences can occur from the grain size of the evaporated gold films or other relatively small imperfections.

All spectra in Figs. 3 and 4 display a broad maximum near λ = 490 nm with peak transmission ≈ 0.15 (≡ 15 %). This peak is from direct transmission of light through the gold film, arising when the real part of the gold dielectric constant is +1 which leads to transparency in the absence of damping, and is not related to any hole or array properties. The peak structure between λ = 560 and 580 nm can be attributed to a combination of a local surface plasmon resonance in each hole and a (1, 1) n_I SPP-BW.

The minima in the spectra for λ > 580 nm can be assigned using the simple predictions of Eq. (1) and Fig. 2. (Note that the Fano resonance feature corresponding to a given SPP-BW occurs as a minimum *and* an adjacent maximum, with the minimum position often closer to the zero-order SPP-BW prediction [3, 5, 7].) For example, when n_{III} = 1.29 < n_I = 1.52 (Fig. 3), B_S = (1, 0) n_{III} SPP-BW is predicted to be at 574 nm and A_S = (1, 0) n_I SPP-BW at 662 nm. These positions are in good agreement with the calculated FDTD minima of 585 and 677 nm as well as the experimental values of 601 nm and 669 nm, respectively. When n_{III} = 1.70 > n_I = 1.52 (Fig. 4), B_S = (1, 0) n_{III} SPP-BW is predicted to be at 733 nm, while the calculated and experimental wavelengths are at 757 nm and 750 nm, respectively. In addition, the A_S = (1, 0) n_I SPP-BW is calculated to be at 669 nm and is observed at 660 nm. When n_{III} = 1.70, the C = (1, 1) n_{III} SPP-BW is predicted to be at 580 nm and is observed in the FDTD and experimental results at 614 nm and 609 nm, respectively.

In thin metal films coupling between SPP-BWs on opposite sides of the film becomes important, especially when n_I is similar to n_{III}. This coupling can produce two new, hybridized SPP-BWs: (1) a high energy anti-symmetric combination and (2) a low energy symmetric combination [14]. The long wavelength peak (symmetric) is red-shifted while the short wavelength peak (anti-symmetric) is blue-shifted relative to the predicted SPP-BW positions from Eq. (1). The amplitudes of the maxima associated with the SPP-BW's also change such that the long wavelength peak has a large amplitude while the short wavelength peak has a small amplitude. Consistent with this general picture, for n_{III} < n_I (where n_{III} = 1.00, 1.29, and 1.40), the hybridized B_S = (1, 0) n_{III} SPP-BW increases in wavelength (from 574 nm to 603 nm to 620 nm) while decreasing in amplitude, and the hybridized A_S = (1, 0) n_I SPP-BW peak near λ = 708 nm increases in amplitude (Fig. 3).

In our discussion so far RAs have not appeared prominently in the calculated or measured transmission spectra because they are generally narrow spectral features (or possibly just kinks [11]) that can be overwhelmed by other processes. For n_{III} > n_I (when n_{III} = 1.60 or 1.70), the maximum to the immediate red of the minimum associated with A_S = (1, 0) n_I SPP-BW shows a rapid rise and narrowing (Fig. 4). This rapid amplitude increase is a direct result of the RA-SPP effect, and calculated transmission spectra on a finer RI scale are shown in Fig. 5. Consistent with Fig. 2, the A_R = (1, 0) n_{III} RA on the top substrate passes through the wavelength region of the A_S = (1, 0) n_I SPP-BW on the glass substrate, coupling with it to produce a narrow, n_{III}-sensitive, spectral feature. Note that owing to partial RA character, the RA-SPP feature occurs close (but still red-shifted) to the zero-order prediction of Eq. (3).

The amplitude variation of the RA-SPP peak in the n_{III} range 1.55 - 1.70 is ≈ 65%/RIU (FDTD) and ≈ 150%/RIU (experiment) (Fig. 5). The difference between the experimental and theoretical amplitude sensitivities is probably from, as noted previously, minor imperfections

#86022 - $15.00 USD Received 1 Aug 2007; revised 15 Nov 2007; accepted 16 Nov 2007; published 19 Dec 2007

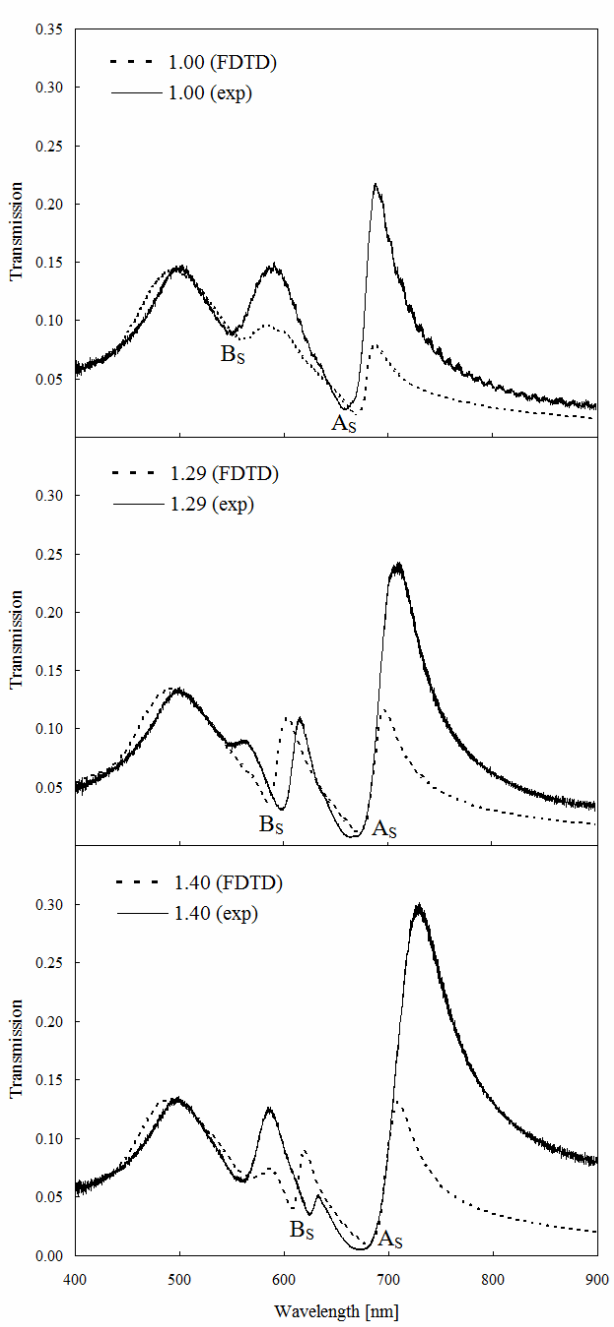

Fig. 3. FDTD and experimental zero-order transmission spectra for $n_{III} < n_I$. The letters are assignments based on Fig. 2.

in the experimental structures. Nevertheless, both simulation and experiment confirm the anticipated large amplitude changes on the basis of the simplified discussion of Fig. 2 and Eqs. (3) and (4). The explicit variation of transmission amplitude with n_{III} could therefore be used to calibrate a system for substrate RI sensing. The wavelength change of a spectral feature with RIU is also sometimes used as a sensing figure of merit. Since the SPP-BW component of the RA-SPP we are focusing on here is, to zero-order, a n_I SPP-BW, we would

#86022 - $15.00 USD Received 1 Aug 2007; revised 15 Nov 2007; accepted 16 Nov 2007; published 19 Dec 2007

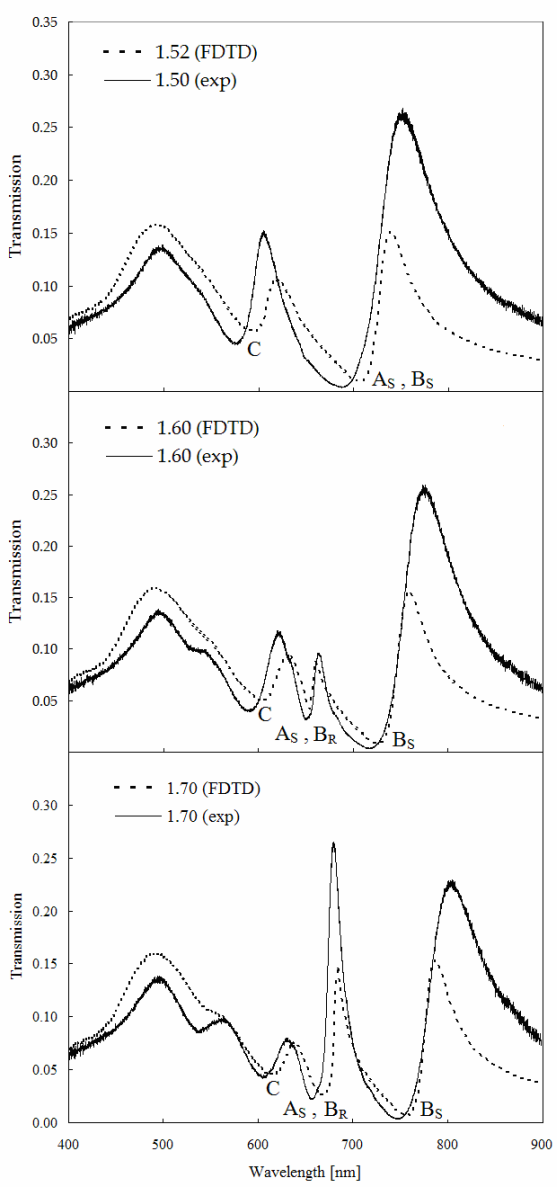

Fig. 4. FDTD and experimental zero-order transmission spectra for $n_{III} \geq n_I$. The letters are assignments based on Fig. 2.

not expect to see much wavelength sensitivity with respect to n_{III}. However, we find that both the calculated and measured wavelength sensitivity of the RA-SPP feature is ≈ 200 nm/RIU, which is mostly due to hybridization effects of the (1, 0) n_I SPP-BW with the (1, 0) n_{III} SPP-BW. Although smaller than values reported for predominantly n_{III}-side SPP-BWs with larger hole periodicities [8], this wavelength sensitivity represents an additional result that can be used in conjunction with the amplitude sensitivity.

To further validate the simplified discussion of the RA-SPP effect, 2D RCWA calculations were carried out. Figure 6(a) shows that RCWA predicts strong variations in zero-order

#86022 - $15.00 USD Received 1 Aug 2007; revised 15 Nov 2007; accepted 16 Nov 2007; published 19 Dec 2007

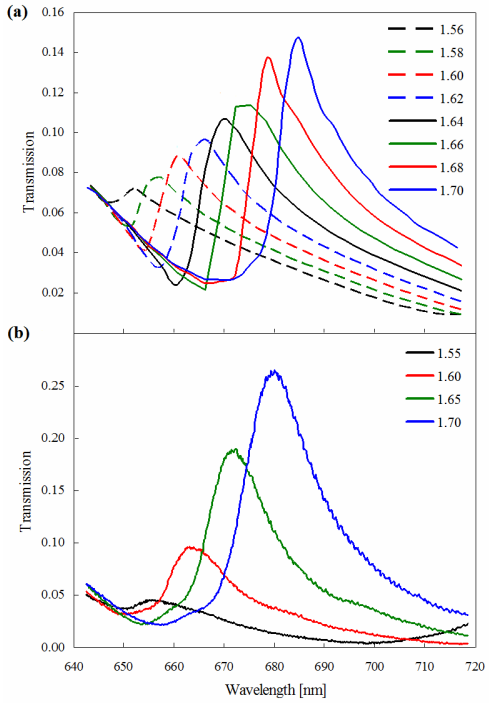

Fig. 5. (a) FDTD calculated zero-order transmission spectra showing a rapid increase in amplitude as n_{III} is varied through the region of the RA-SPP. (b) Experimental results consistent with (a).

transmission with changing n_{III} in agreement with 3D FDTD and experimental trends. In addition, the RCWA method reveals that first-order diffraction is also significantly enhanced by the RA-SPP effect, Fig. 6(b). As expected, first-order diffraction, dominated by the (1, 0) n_{III} RA, exhibits a wavelength sensitivity equal to the theoretical upper limit, *P*/RIU. RCWA calculations were carried out over a wide range of periodicities and n_I values to confirm that the rapid variations in transmission amplitude are always consistent with the predictions of Eqs. (3) and (4). Further RCWA calculations revealed that the RA-SPP effect persists strongly for film thicknesses up to 65 nm and is more pronounced with the use of larger slit widths. For example, the amplitude variation with RIU almost doubles when the slit width is increased to 175 nm.

3.3 Field profiles

Here we examine FDTD calculated field profiles to verify coupling between the (1, 0) n_{III} RA and (1, 0) n_I SPP-BW. Figure 7 shows the frequency-resolved *z* component of the electric field, $|E_z|^2$, for λ = 679 nm (near the RA-SPP crossing point) with n_{III} = 1.70. Figure 7(a) shows that the (1, 0) n_I SPP-BW has greatest intensity on the n_I side, but also some noticeable intensity on the n_{III} side. The (1, 0) n_{III} RA is present but is not visible in this plot since its intensity relative to the (1, 0) n_I SPP-BW is small. However, Fig. 7(b) is the field for $z > 200$ nm and shows characteristic RA features, i.e., an extended propagating plane wave [15]. The high intensity of (1, 0) n_{III} RA near the film interface, which decreases in strength as the distance from the film increases, suggests that the (1, 0) n_{III} RA is coupled to the (1, 0) n_I SPP-BW.

#86022 - $15.00 USD Received 1 Aug 2007; revised 15 Nov 2007; accepted 16 Nov 2007; published 19 Dec 2007

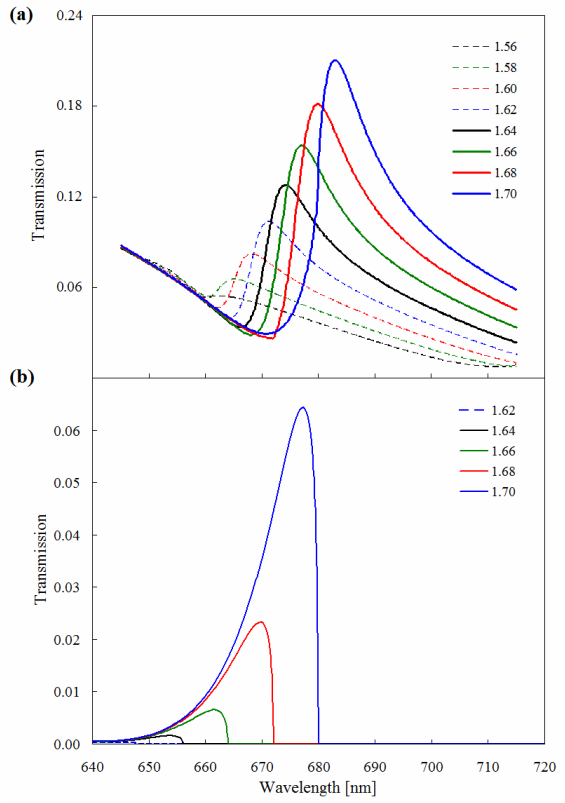

Fig.6. RCWA calculations of the (a) zero and (b) first-order transmission as n_{III} is varied through the region of the RA-SPP.

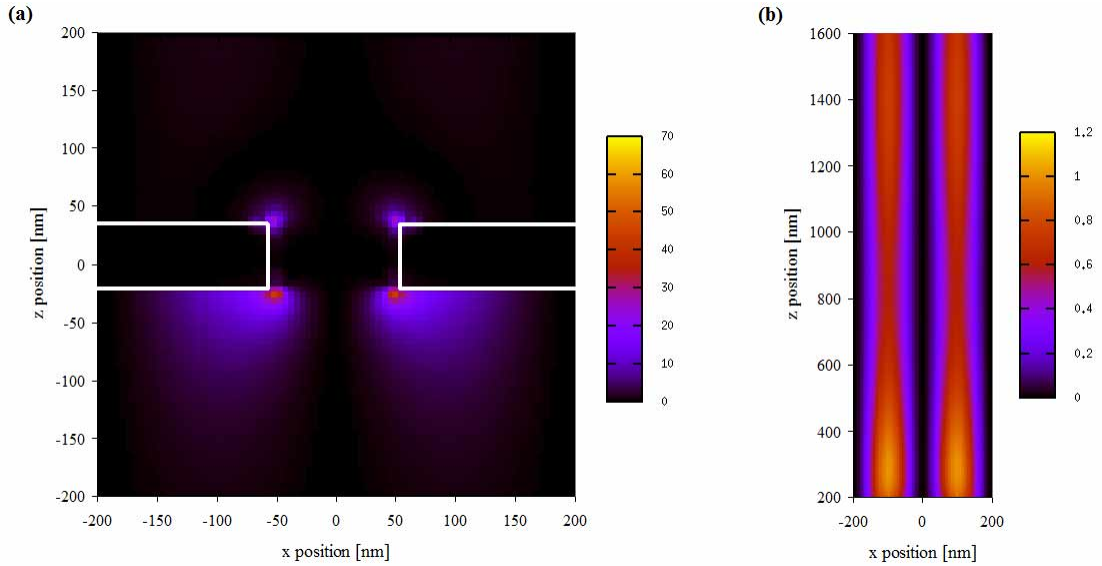

Fig. 7. FDTD calculated frequency resolved $|E_z|^2$ at λ = 679 nm with n_{III} = 1.70: (a) region near the hole and (b) 200 nm above the gold film. The hole is centered at the origin and the film boundaries are outlined in white.

#86022 - $15.00 USD Received 1 Aug 2007; revised 15 Nov 2007; accepted 16 Nov 2007; published 19 Dec 2007

4. Concluding remarks

In summary, we have presented a theoretical and experimental study of light transmission through periodic hole arrays in thin gold films that demonstrates an approach for using these systems for RI sensing. In particular, the coupling of a SPP-BW on the one side of the film with a RA on the other, which we term the RA-SPP effect, leads to a large increase in transmission of a narrow linewidth peak over a small RI range. Furthermore, we presented simple relations to estimate the structural and material parameters of the system necessary to observe this effect near a specified RI value. The characterization of such features provides new chemical sensing capabilities for hole array systems that complements existing approaches [8, 16].

Acknowledgements

GCS and JMM were supported by the US Department of Energy under grant No. DEFG02-03-ER15487 and the Northwestern Materials Research Center, sponsored by the National Science Foundation (DMR-0520513). TWO and JH were supported by the NSF under awards DMR-0632947 and DMR-0705741. SKG was supported by the U.S. Department of Energy, Office of Basic Energy Sciences, Division of Chemical Sciences, Geosciences, and Biosciences under contract DE-AC02-06CH11357. This research used resources of the National Energy Research Scientific Computing Center, which is supported by the Office of Science of the U.S. Department of Energy Contract DE-AC02-05CH11231.

#86022 - $15.00 USD Received 1 Aug 2007; revised 15 Nov 2007; accepted 16 Nov 2007; published 19 Dec 2007